

Coupled Models of Brittle-plastic Deformation and Fluid Flow: Approaches, Methods, and Application to Mesoproterozoic Mineralisation at Mount Isa, Australia

Klaus Gessner

Received: 31 July 2008 / Accepted: 27 February 2009 / Published online: 4 April 2009
© Springer Science+Business Media B.V. 2009

Abstract Rock deformation has an important effect on the spatial distribution and temporal evolution of permeability in the Earth's crust. Hydromechanical coupling is of fundamental significance to natural fluid–rock interaction in porous and fractured hydrothermal systems, and in the assessment and production of hydrocarbon resources and geothermal energy. Shearing and fracturing of rocks can lead to the creation or destruction of permeability when fractures or faults form, or when existing structures are reactivated. Changes in stress orientation or fluid pressure can drive rock failure and create dilating fault zones that have the potential to focus fluid flow, or to breach seals above overpressured fluid compartments. Here, numerical models of deformation and fluid flow related to Mesoproterozoic copper mineralisation at Mount Isa, Australia, are presented that show how changes in deformation geometry in multiply deformed geological architectures relate to changes in dilation patterns, fluid pathways and flow geometry. Coupled numerical simulations of deformation and fluid flow can be useful tools to better understand structural control on fluid flow in hydrothermal mineral systems.

Keywords Hydrothermal systems · Faults · Fluid flow · Permeability · Mount Isa · Copper · Hydrothermal ore deposits · Australia · Numerical models

1 Introduction

Tectonic processes in the Earth's lithosphere create and destroy fluid pathways by modifying porosity and permeability. It is through this mechanical and thermal modification of hydraulic architecture that hydrothermal fluid flow is fundamentally related to the spatial and temporal availability of permeable structures in the Earth's crust. Consequently, the

K. Gessner (✉)
Centre for Exploration Targeting, School of Earth and Environment, The University of Western Australia, 35 Stirling Highway, Crawley, WA 6009, Australia
e-mail: Klaus.Gessner@uwa.edu.au

K. Gessner
CSIRO Exploration and Mining, 21 Dick Perry Avenue, Kensington, WA 6102, Australia

evolution of fluid pathways in space and time exerts a fundamental control on the occurrence of mineral and hydrocarbon resources, and geothermal systems. In addition to modelling heat transfer, fluid flow and reactive transport, numerical simulations can also be used to model the feedback between rock deformation and fluid flow, in particular the spatial control of an emerging hydraulic architecture on the flow geometry. This article contains a brief outline of basic relations between rock deformation and fluid flow in the frictional-plastic regime, followed by an example of the application of mechanical-fluid flow coupled numerical simulations related to hydrothermal copper mineralisation at Mount Isa, Australia. In the Mount Isa example, different strain geometries were applied to a complex, multiply deformed geological architecture, and it is shown how the spatial distribution of plastic dilation leads to the generation of different fluid pathways.

This article is based on material presented during the short course ‘Process modelling of hydrothermal systems’ at RWTH International Academy in Aachen, Germany in 2006, 2007, and 2008.

2 Deformation and Fluid Flow in the Brittle Crust

Coupling between the physical processes in hydrothermal systems and the geological architecture are complex, and some of the most important interactions occur between rock deformation and fluid flow. Deformation processes and fluid flow drivers vary within the Earth’s crust due to their dependency on pressure, temperature, physical properties of rocks and fluids, and the geometric characteristics of hydraulic conductivity on different scales. In essence the relation between rock deformation and fluid flow depends on how elastic, plastic and viscous deformation processes interact with processes that drive fluid flow, such as buoyancy and spatial gradients in hydraulic head. Deformation processes in turn depend on the temperature, pressure and composition of rocks. This is of particular significance at deep levels of the Earth’s crust, where fluid flow is highly dependent on net volume changes in fluid from metamorphic and magmatic sources, while the permeability is closely tied to grain-scale porosity created by metamorphic reactions or crystal-plastic deformation processes (e.g. Ague 2004, and references therein). The interaction between porous flow and predominantly elastic deformation at shallow levels of the Earth’s crust is expressed by the term hydromechanical coupling (e.g. Neuzil 2003; Rutqvist and Stephansson 2003). Hydromechanical coupling addresses the modification of pore space in a deforming rock mass, but also the fracturing and shearing of rocks caused by pressure changes. In specific geological situations hydromechanical interaction can lead to a drastic modification of the hydraulic architecture, such as the localisation of new faults, fault reactivation, and the breaching of seals (e.g. Sibson 1994). The consideration of heat transfer in addition to deformation and fluid flow—thermo-hydromechanical coupling—has allowed researchers to better understand the heat budget, and the role of thermo-elastic effects in natural and engineered geothermal systems (e.g. Kolditz and Clauser 1998; Ghassemi et al. 2007).

2.1 Volume Change During Deformation

In the brittle crust, deformation often leads to volume change in rocks. Faults and fractures exert a tight spatial control on fluid flow, because of their ability to inhibit or to enhance permeability. Deformation induced permeability, or dynamic permeability, modifies the intrinsic permeability of a rock mass by changing the volume and shape of its pore space.

The deformation induced change of porosity and permeability is a consequence of elastic and plastic behaviour of the rock mass. Plasticity can occur in the form of compaction of under-consolidated porous rocks, slip along fractures, and crystal-plastic deformation mechanisms. The distinction between volume change due to fracturing or dilation of a continuum is often based on the scale of observation. These scales of observation translate directly to the question how to model the relation between rock deformation and fluid flow at a given scale: by using a continuum approach, or a discrete approach. Clauser (1992) has shown that although intrinsic permeability in crystalline rocks is scale-sensitive, permeability values do not increase continually towards large scale. In contrast to scaling laws based on single fractures, which infer a cubic relation between fracture width and volumetric flow rate (e.g. Cook et al. 1990), permeability values increase with measurement scale, but reach a maximum on the metre to 100-m measurement scale before decreasing again at larger scales (Clauser 1992). These findings suggest that porous media are a valid approximation for modelling volumes of fractured rocks.

When a rock deforms as an elastic solid, an increase in the stress difference generally leads to volume loss of the solid (e.g. Edmond and Paterson 1972; Mandl 1988; Paterson and Wong 2005). The amount by which the solid volume changes during elastic deformation, varies according to rock type, and can be quantified by determining the elastic properties of the rock. Plastic failure of rock, however, often leads to much larger volumetric strain, which can be expressed either as volume increase (dilation), or decrease (compaction), depending on rock type and confining pressure. Neuzil (2003) and Rutqvist and Stephansson (2003) published detailed reviews on hydromechanical coupling in geological, and engineered systems with a focus on poroelasticity and plasticity in the form of compaction of under-consolidated sediments. Compaction is often observed in under-consolidated sediments and sandstones (Aydin and Johnson 1983; Fisher and Knipe 1998; Sheldon et al. 2006), while dilation is more likely in crystalline and metamorphic rocks, particularly at the onset of deformation and at low confining pressure (e.g. Edmond and Paterson 1972; Fischer and Paterson 1989; Hobbs et al. 1990; Ord 1990; Ord and Oliver 1997; Zhang et al. 1994; Paterson and Wong 2005). Deformation induced volume change can either be expressed by a modification of the porosity and permeability of a continuous rock volume, or by the generation of a fracture-rock discontinuum. Fractured rock is of particular interest in groundwater flow, hydrothermal ore deposits and geothermal systems because interconnected fractures provide high hydraulic conductivity (e.g. Secor 1965; Secor and Pollard 1975), with the potential for high fluid flow rates which favour the advection of heat and chemical species in solution. Fracture zones are also important for some fluid-dominated hydrothermal ore deposits, because they can provide the space to precipitate minerals in economic concentration and quantities (e.g. Oliver and Bons 2001). For continuous aggregate materials such as rock, soil or concrete, dilation can be expressed as the dilation angle (Vermeer and de Borst 1992), which quantifies volume increase of a continuum during plastic deformation (Ord and Oliver 1997).

2.2 Hydrofracturing

Deformation of the Earth's crust occurs when stress exceeds rock strength. In the brittle crust, rock behaves as a frictional plastic solid, i.e. its strength increases with increasing pressure (e.g. Coulomb 1773; Mohr 1900; Byerlee 1978; Jaeger and Cook 1979). Stress is defined as force per unit area, and is expressed in three dimensions as a second order tensor (e.g. Jaeger and Cook 1979; Twiss and Moores 1992). For each arbitrary orientation of a plane in a rock volume, stress can be decomposed into normal and shear components on

that plane. In each volume of rock one orientation of mutually orthogonal planes exists, where shear stresses are zero, and normal stresses are at maximum values. The directions normal to these planes are called the principal stress axes. The natural state of stress in the Earth's crust is triaxial, i.e. the values for the three principal stress axes are different. By convention the stress axes are named σ_1 , σ_2 and σ_3 for the largest, the intermediate, and the smallest value respectively, and it is the difference between σ_1 and σ_3 , or stress difference, that affects rock strength. Stress values can be positive (compressive) or negative (tensile). Stress difference can be caused by gravity, tectonics, or changes in pore pressure. In addition to increasing stress difference, rock failure in shear or tension can also be achieved by increasing fluid pressure in the pore space and thus lowering effective stress (e.g. Hubbert and Rubey 1959; Handin et al. 1963; Secor 1965; Jaeger and Cook 1979). For the frictional-plastic deformation regime the relation between pressure and the stress tensor can be visualized in a Mohr diagram (Fig. 1). Hydromechanically driven failure occurs, because the pore fluid has a load-bearing capacity. Conceptually, fluid pressure can be expressed as having the same value in all directions and therefore counteracting normal stress components of a framework of grains surrounding a pore in all directions. Values along all three principal stress axes are therefore reduced in the same quantity. The 'wet' reduced stress state is referred to as effective stress, the 'dry' stress state as applied stress. Tensional failure caused by the increase of pore pressure, or hydrofracturing, is a common reservoir engineering practice in well stimulation. The natural occurrence of hydrofracturing has been associated with the release of fluids during prograde metamorphic conditions at mid-crustal levels (Etheridge et al. 1984), as well as the formation of many structurally controlled breccia-hosted and vein-hosted ore deposits (e.g. gold; Nguyen et al. 1998; Cox et al. 2001; Sibson 2001).

2.3 Fluid Pressure Gradients

Fluid pressure levels in the crust are subject to the balance between fluid production and permeability at different levels of the Earth's crust. Substantial spatial variations of fluid pressures result in hydraulic head gradients that can have a significant impact on the vertical component of fluid flow. If more fluid is produced in the rock column than can be drained, e.g. due to compaction of sediments, the production of fluid during metamorphic reactions, or the release of fluids from crystallizing magma, fluids can become pressured at higher values than in a case where they have a free surface at the Earth's surface. The pressure of a fluid at rest is determined by

$$p = \rho gz \quad (1)$$

where p is pressure, ρ density, g gravitational acceleration, and z depth. The increase of pressure with depth is determined by the gradient $\frac{dp}{dz}$, which is called hydrostatic for water and lithostatic for rock densities (Fig. 2). When low permeability inhibits fluid flow, any produced fluid will cause pressure to increase to values between hydrostatic and lithostatic. Fluids subject to higher than hydrostatic gradients will be driven upward due to the overpressure, and although this is a transient phenomenon, the low permeability of clays, shales, and crystalline rocks can lead to the existence of overpressured fluid reservoirs over geological time scales.

Increasing pressure in sealed reservoirs, and also in re-cemented fault rocks, can lead to fracturing and transient fluid flow (Matthäi and Roberts 1997; Braun et al. 2003; Sheldon and Ord 2005). Due to the ubiquitous evidence for fluid flow down gradients of

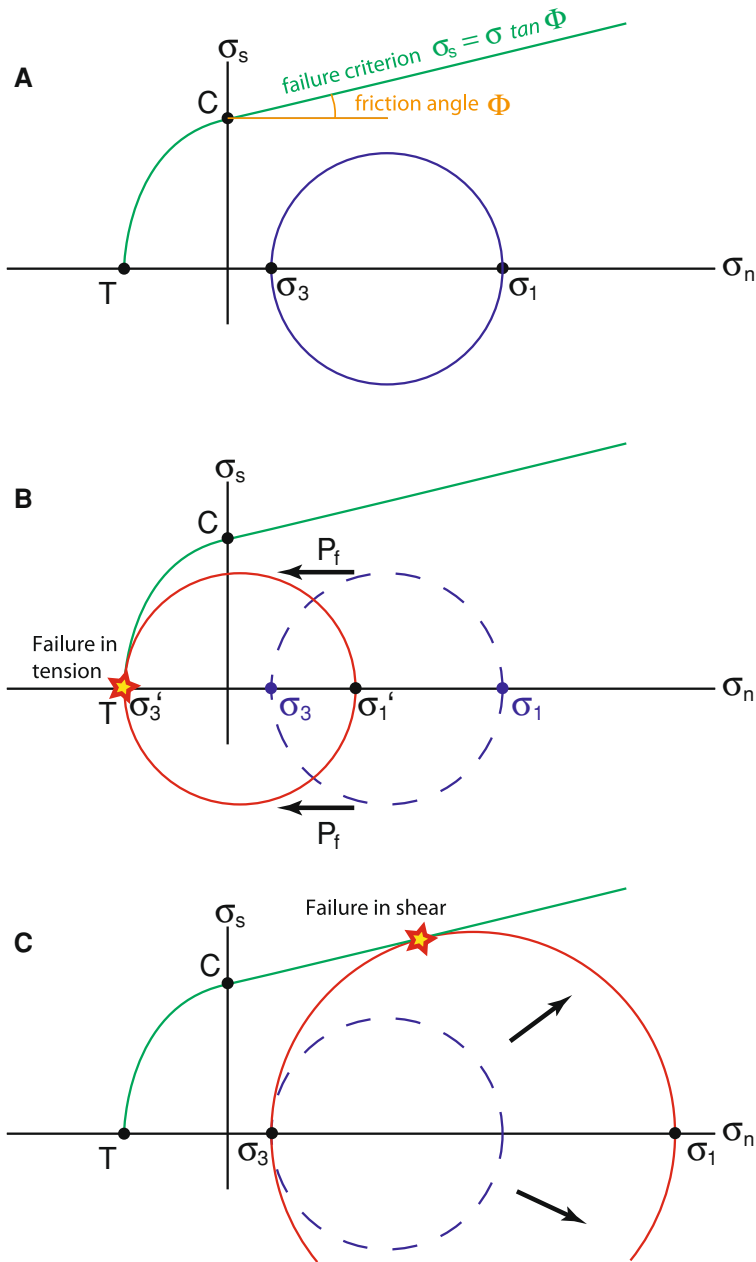
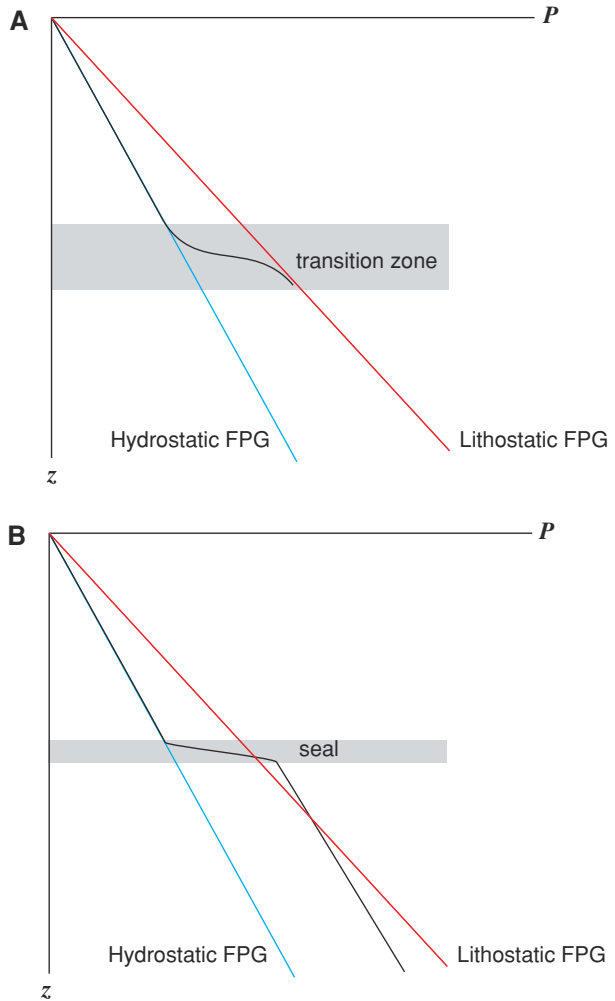


Fig. 1 Failure modes for frictional-plastic rocks in a Mohr diagram. **a** Shows shear and normal components of major and minor principal stress axes σ_1 and σ_3 , and failure curve (green) for a material with a cohesion C , a tensile strength T , and a friction angle Φ ; failure is shown as a combination of Mohr envelope and Coulomb's linear failure criterion; **b** Shows reduction of 'applied' triaxial stress with low stress difference by fluid pressure ('effective stress') and consequent failure in tension; **c** shows failure in shear due to increasing the stress difference. Notice that increasing fluid pressure when the stress difference is large can also lead to failure in shear

Fig. 2 Fluid pressure gradients (after Cox 2005). **a** Transition from hydrostatic to lithostatic in sedimentary basins across a fluid overpressured transition zone; **b** overpressured fluid reservoir at hydrostatic gradient below a seal. In both cases there is a potential to drive flow upward in regions where fluid pressure departs from hydrostatic gradient, but the high pore pressure below the seal (in **b**) may favour tensile failure of the rock at the top of the reservoir



temperature and pressure in hydrothermal gold deposits associated with quartz-veins, the release of mineralising fluids from overpressured reservoirs by hydrofracturing of the seal is a commonly applied model for structurally controlled fluid flow at the base of the brittle crust (e.g. Etheridge et al. 1984; Sibson 1994, 2001; Cox et al. 2001; Nguyen et al. 1998; Cox 2005). For detailed reviews on this subject the reader is referred to Cox et al. (2001), Sibson (2001), Cox (2005), and Yardley and Baumgartner (2007).

2.4 Modelling Approaches

To model the structural control on hydrothermal fluid flow a number of approaches exist. One approach is based on the concept that permeability increase is caused by the mechanical loading of rock around the slip plane of a fault. The local increase of stress difference during the mechanical loading of the model is therefore used as proxy for the spatial distribution of permeable regions, and fluid flow as such is not simulated. Models

are either purely elastic (Cox and Ruming 2004; Micklethwaite and Cox 2004), based on damage mechanics concepts (Sheldon and Micklethwaite 2007), or simulate plasticity by slip along interfaces of discrete elements representing weak fault systems (Ojala et al. 1993; Holyland and Ojala 1997; Mair et al. 2000). Other workers have used numerical models based on coupling Mohr–Coulomb plasticity with Darcy flow as implemented in the finite difference codes FLAC (Itasca 2000) and FLAC^{3D} (Itasca 2003; Cundall and Board 1988), to simulate dilation in complex multi-material geometries (Jiang et al. 1997; Gow et al. 2002; Oliver et al. 2001; Ord et al. 2002; Ord and Oliver 1997; Schaubs and Zhao 2002; Sorjonen-Ward et al. 2002; Gessner et al. 2006; McLellan et al. 2004; Sheldon and Ord 2005; Robinson et al. 2006; Schaubs et al. 2006; Vos et al. 2007; Zhang et al. 2006a, b, 2007; Potma et al. 2008). The latter technique is based on coupling Darcy flow to a Mohr–Coulomb constitutive model including plasticity. Advantages of the latter technique lie in the capability to simulate plasticity due to localisation of deformation (Hobbs et al. 1990; Ord 1990), the spatial mechanical response of a given 3D rock property distribution to tectonic stress, and the change of permeability linked with volume strain. Coupled modelling of Mohr–Coulomb plasticity and Darcy flow has proven useful in understanding deformation driven fluid flow at the mine to district scale, where a number of different rock types occur in a particular geological architecture. Schaubs et al. (2006) and Potma et al. (2008) have shown how this method can be successfully applied as a tool for target generation in mineral exploration. Ideally, in validation stage, the impact of different strain geometries on dilation and fluid flow is tested against known alteration and mineralisation patterns in a data rich location, before being applied for exploration in data poor areas.

3 Mount Isa Copper Case Study

This section comprises an example of deformation and fluid flow coupled modelling of Mohr–Coulomb plasticity with Darcy flow, as described in the previous section. The objective of the modelling was to investigate how the deformation geometry relates to patterns of mineralisation and alteration within the Mesoproterozoic Mount Isa Copper deposit in northwest Queensland, Australia.

3.1 Geological Background

The Mount Isa lead–zinc–silver and copper deposits are located in the Mount Isa Inlier, an inverted and metamorphosed Proterozoic intra-continental rift (Betts et al. 2006) in North-West Queensland, Australia (Fig. 3). The Urquhart Shale, which hosts both the lead–zinc–silver and the copper mineralisation, is part of the Mount Isa Group, a Mesoproterozoic series of carbon-rich siliciclastic sediments and carbonates, which were deposited during a sag-phase following the third major rifting event in the Mount Isa Inlier (Betts et al. 2006). A number of detailed studies (Bell et al. 1988; Perkins 1984; Swager 1985) concluded that copper ore was deposited after the main tectono-metamorphic events of the Isan Orogeny, and postdates the lead–zinc–silver mineralisation at the same location. According to recent geochemical studies (Wilde et al. 2005; Gregory et al. 2005; Kendrick et al. 2007) alteration and copper mineralisation involved several fluids, including an upward flowing basement-equilibrated reduced fluid, and an oxidised brine originating from near-surface reservoirs. Structural work in the mine and its vicinity outlined three major deformation events during the Isan orogeny: D2 E–W shortening, D3 top-to-E simple-shear, and D4

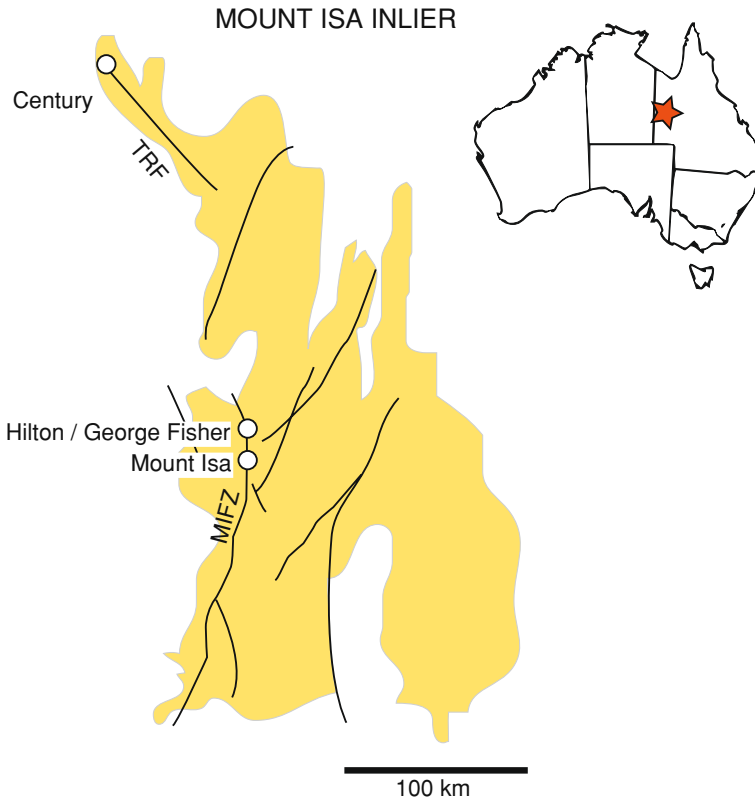


Fig. 3 Location of Mount Isa (Pb–Zn–Ag, Cu), Hilton/George Fisher (Pb–Zn–Ag), and Century (Pb–Zn–Ag) Mines in Mount Isa Inlier. Also shown are major fault systems, including Termite Range Fault (*TRF*), and Mount Isa Fault Zone (*MIFZ*)

dextral oblique slip (Bell and Hickey 1998; Connors and Lister 1995; Connors et al. 1992). The basal part of the Urquhart shale, located immediately above metamorphosed basalts and sediments of the Eastern Creek Volcanics (Fig. 4) displays the most intense fracturing and the highest ore grade of up to 25% copper. The contact is a folded, and in parts reactivated, fault zone known as the Paroo Fault.

3.2 Method

To model deformation and fluid flow in the Mount Isa copper system, the finite different code $\text{FLAC}^{3\text{D}}$ (Itasca 2003) was used. The algorithm solves the governing equations of mass, momentum and single phase saturated flow. Mathematical background, governing laws, constitutive laws and their implementation are documented in detail in the software manual (Itasca 2003), but will be summarized here.

3.2.1 Deformation

The law governing the motion of an elementary volume as a response to the forces applied is expressed as Cauchy's equation of motion

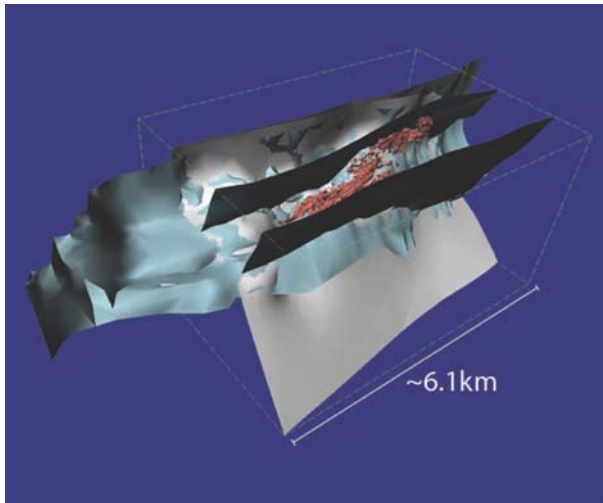


Fig. 4 3D model of Mount Isa Copper deposit, where the *light grey* surface represents an extrapolation of Paroo fault from mine data (*light blue* surface). Ore containing more than 2.5% Cu is shown in *red*. *Dark* surfaces outline upper (*back*) and lower (*front*) stratigraphic boundaries of Urquhart Shale. View is toward NW, and down

$$\sigma_{ij,j} + \rho b_i = \rho \frac{dv}{dt} \quad (2)$$

where $\sigma_{ij,j}$ is the partial derivative of the stress components across the coordinate planes with respect to x_j , ρ is mass per unit volume, b body force per unit mass, and $\frac{dv}{dt}$ the material derivative of velocity.

To simulate deformation, isotropic and anisotropic Mohr–Coulomb constitutive models have been chosen, where shear- and tension yield functions determine the shape of the failure envelope, with a non-associated flow rule for former, and by an associated flow rule for the latter type of yield:

Isotropic materials

shear failure criterion

$$f^s = \sigma^1 - \sigma^3 \frac{1 + \sin(\phi)}{1 - \sin(\phi)} + 2c \sqrt{\frac{1 + \sin(\phi)}{1 - \sin(\phi)}} \quad (3)$$

shear flow law

$$g^s = \sigma^1 - \sigma^3 \frac{1 + \sin(\psi)}{1 - \sin(\psi)} \quad (4)$$

tension failure criterion

$$f^t = \sigma^3 - \sigma^t \quad (5)$$

tension flow law

$$g^t = -\sigma^3 \quad (6)$$

Anisotropic materials

shear failure criterion

$$f^s = \tau + \sigma_{33} \tan \phi_j - c_j \quad (7)$$

shear flow law

$$g^s = \tau + \sigma_{33} \tan \psi_j \quad (8)$$

tension failure criterion

$$f^t = \sigma_{33} - \sigma'_j \quad (9)$$

tension flow law

$$g^t = \sigma_{33} \quad (10)$$

Here ϕ is the friction angle, ϕ_j the weak plane friction angle, c cohesion, ψ the dilation angle, ψ_j the weak plane dilation angle, and τ one of four components of the stress vector describing weak-plane failure (the other three being σ_{11} , σ_{22} and σ_{33}).

3.2.2 Fluid Flow

The law governing fluid transport is given by Darcy's law in the form

$$q_i = -k_{ij} \hat{k}(s) [p - \rho_f x_j g_j]_i \quad (11)$$

Here, q_i is specific discharge, k the absolute mobility tensor (permeability, as implemented in FLAC^{3D}), $\hat{k}(s)$ the relative mobility coefficient (a function of the saturation s), p is pore pressure, ρ_f is fluid density, and g gravity. The constitutive law used to describe the response of pore fluid to pore pressure, saturation and mechanical volume strain, ε , is

$$\frac{1}{M} \frac{\partial p}{\partial t} + \frac{n}{s} \frac{\partial s}{\partial t} = \frac{1}{s} \frac{\partial \zeta}{\partial t} - \alpha \frac{\partial \varepsilon}{\partial t} \quad (12)$$

where M is Biot modulus, ζ the variation of fluid content, and α Biot coefficient (Biot 1956).

3.2.3 Implementation

In FLAC^{3D} the model domain is discretised into brick shaped zones that consist of tetrahedral subdomains ('mixed discretisation procedure', Marti and Cundall 1982). In the simulations, the algorithm solves paralleled nodal formulations of the deformation and fluid flow equations in an explicit time-marching scheme (Itasca 2003).

3.3 3D Mine-Scale Model

To investigate the critical factors for providing strain localisation and increased permeability at the mine scale a number of simulations of deformation and fluid flow have been carried out using *FLAC*^{3D}. In particular it was important to investigate if different deformation scenarios would control the vertical component of fluid flow, and the localisation of deformation and the focussing of fluid flow at the site of mineralisation in the Urquhart shale. The vertical component of fluid flow is important, because upward and downward flow can be related to different alteration assemblages (Wilde et al. 2005). All simulations are based on a structured mesh (Fig. 5) containing 54,021 brick shaped elements of equal size with 49 each in *x* (N–S) and *y* (E–W), and 21 in *z* (vertical), and dimensions of *x* = 6,098 m, *y* = 5,428 m and *z* = 2,973 m. The mesh was generated from geologic maps, and exploration and mine datasets. The models were simulated fully saturated and initialised at either hydrostatic, or 50% lithostatic fluid pressure gradients, and with impermeable boundaries. Following the estimate of Heinrich et al. (1993) who estimated ca. 5 km depth during copper ore formation, the top of the model was assumed to be at a depth of 4,500 m, the bottom at 7,473 m. Regions of elements in the model define stratigraphic rock units and faults, to which material properties were assigned. These properties were modified from literature values (Itasca 2000) for shale, siltstone, schist and basalt to reflect relative lithological variations of the local geology (Table 1). In general the faults were assumed to be weaker and more permeable than rock units. Deformation-related permeability change was accounted for by linking post-failure plastic dilation to a permeability increase, as well as by assuming a five-fold increase in permeability during failure in tension, and a two-fold permeability increase relative to the undeformed rock after tensional failure. For most models strength variations within the Mount Isa Group

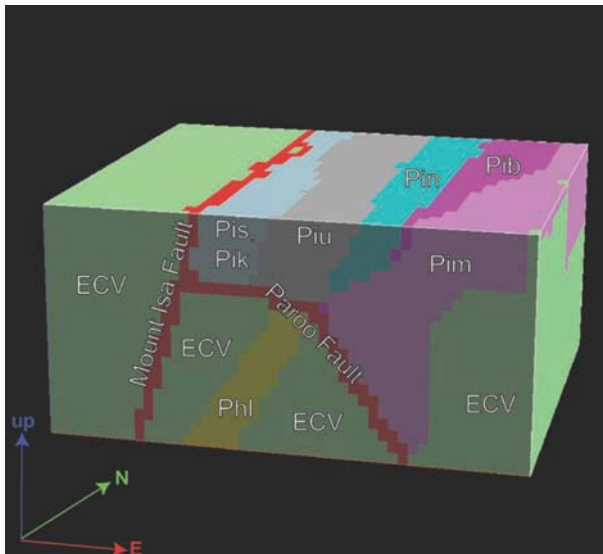


Fig. 5 Mesh used in the numerical simulations showing faults and rock units. *ECV* = Eastern Creek Volcanics, *Phl* = Lena Quartzite, *Pim* = Moondarra siltstone, *Pib* = Breakaway shale, *Pin* = Native Bee siltstone, *Piu* = Urquhart shale, *Pis*, *Pik* = Spear and Kennedy siltstones; see Fig. 7 for scale

Table 1 Material properties used in the 3D mine-scale model

Unit	Density (kg m^{-3})	Bulk modulus (Pa)	Shear modulus (Pa)	Friction angle ($^\circ$)	Cohesion (Pa)	Dilation angle ($^\circ$)	Tensile limit (Pa)	Permeability (m^2)
Eastern Creek Volcanics	3500	2×10^{10}	9×10^9	30	5.5×10^7	7	1.31×10^7	1×10^{-16}
Lena Quartzite	2700	3.8×10^{10}	1.3×10^{10}	48	7×10^7	10	1×10^7	1×10^{-15}
Faults	2700	2.7×10^{10}	7×10^9	28	2.7×10^7	12	1.2×10^6	5×10^{-15}
Moondarra siltstone	2700	1.6×10^{10}	1.1×10^{10}	32	3.5×10^7	10	3×10^6	2×10^{-16}
Breakaway shale	2700	8×10^9	4×10^9	15	3.5×10^7	5	1.4×10^7	1×10^{-16}
Native Bee siltstone	2700	1.6×10^{10}	1.1×10^{10}	32	3.5×10^7	10	3×10^6	2×10^{-16}
Urquhart shale	2700	3.23×10^{10}	6.5×10^9	$20/10^a$	$4 \times 10^7/2 \times 10^{6a}$	$5/5^a$	$9 \times 10^6/4.5 \times 10^{6a}$	6×10^{-16}
Kennedy Spear siltstone	2700	1.6×10^{10}	1.1×10^{10}	32	3.5×10^7	10	3×10^6	2×10^{-16}

^a Property values used for the weak direction in the anisotropic constitutive model

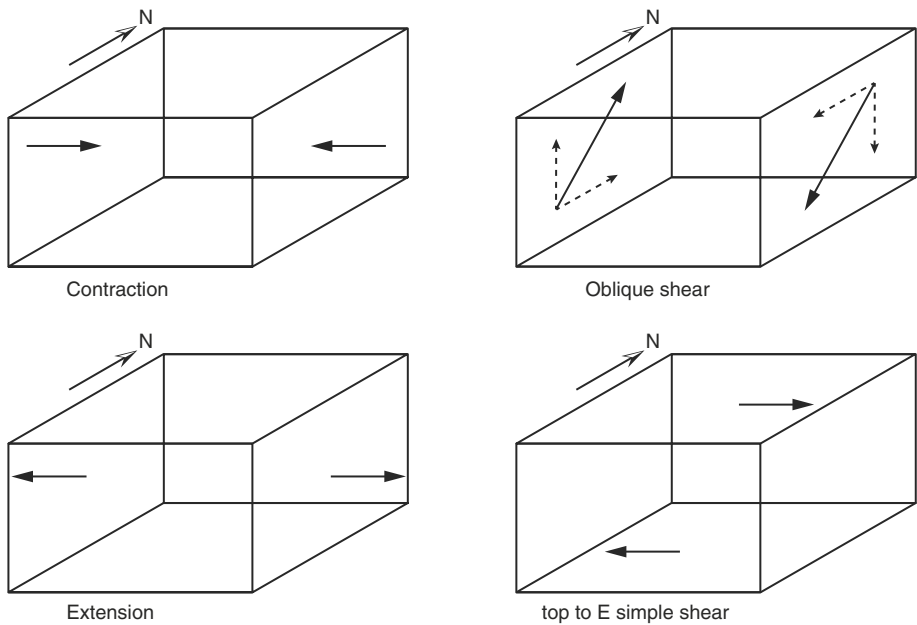


Fig. 6 Geometry of velocity boundary conditions applied to the grid

sediments have been estimated according to their mica and quartz content, with the Eastern Creek Volcanics in the basement being modelled as the least permeable and strongest rocks. To account for the different tectonic events, syn- to post D_2 , E–W contraction, oblique dextral strike slip, extension, and top-to East simple shear strain geometries were simulated (Fig. 6). Contraction models were run to 5% shortening and extension models to 5% extension. The oblique strike slip models were run to a vertical shear angle of $\psi = 0.68^\circ$ and a horizontal shear angle of $\psi = 0.85^\circ$; the top-to East simple shear models were deformed to $\psi = 0.11^\circ$. Deformation was applied by imposing a displacement field across the nodes of the finite difference grid. Based on field observations the Urquhart shale needed to be modelled as an anisotropic rock. Since at the scale of the model the Urquhart shale's layering could not be resolved, its anisotropy was accounted for by assuming a weak plane in the orientation of bedding ('ubiquitous joints' constitutive model, as described above). This means that the rock has less strength in a 60° W-dipping orientation, and shears more easily along that plane. According to the anisotropy, the weak layers would be expected to control the overall deformation behaviour of the Urquhart shale. Shear strain along the plane of the anisotropy was therefore used as a proxy for tensile failure in the siltstone layers.

3.4 Modelling Results

The key observations from these models can be summarised as follows:

1. *In contraction* simulations strain localises along the lower, E-dipping part of the Paroo fault. From this E-dipping reverse-sense shear zone a W-dipping, reverse-sense secondary shear zone nucleates in the lower part of the Urquhart shale (Fig. 7). Fluid flow patterns are dominated by upward flow and focusing into the dilating regions,

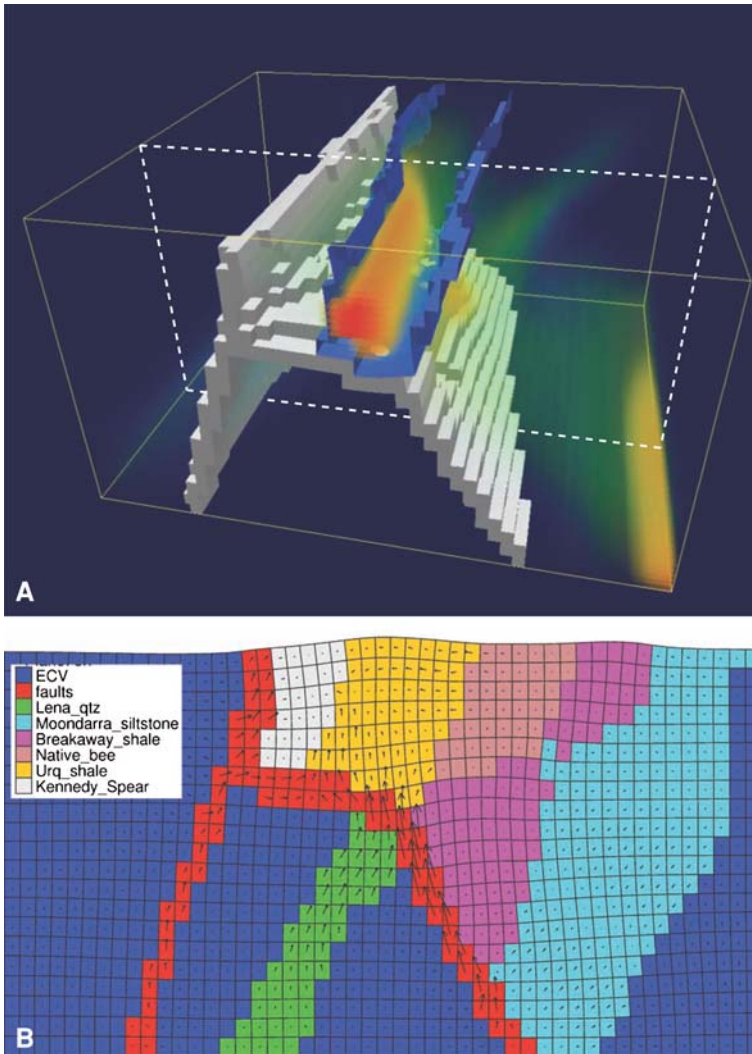


Fig. 7 E–W contraction scenario. **a** Strain pattern where shear strain maximum in *red*, lower values *yellow* to transparent. Paroo and Mount Isa fault are outlined in *grey*, boundaries of Urquhart shale in *blue*. View is towards N; position of cross section in **b** is shown by *white dotted line*. **b** Fluid flow field at 5% contraction along an E–W section in the centre of the model. Notice focused upward flow in the faults (*red*), the Lena Quartzite (*green*), and into the base of the Urquhart shale (*yellow*)

particularly the Urquhart shale. In all contraction cases flow is upward, and becomes focussed in the Paroo Fault, the Mount Isa Fault, the Urquhart shale, and the Lena Quartzite with a maximal velocity of $9 \times 10^{-8} \text{ ms}^{-1}$ (ca. 3 m/year).

2. In *oblique strike slip* simulations a range of steep NNE–SSW trending dextral shear zones form, and the Mount Isa fault becomes reactivated. Tensile failure occurs in the Eastern Creek Volcanics close to the Mount Isa fault, the Lena Quartzite, and is inferred from shear along the anisotropy of the Urquhart shale (Fig. 8). The fluid flow

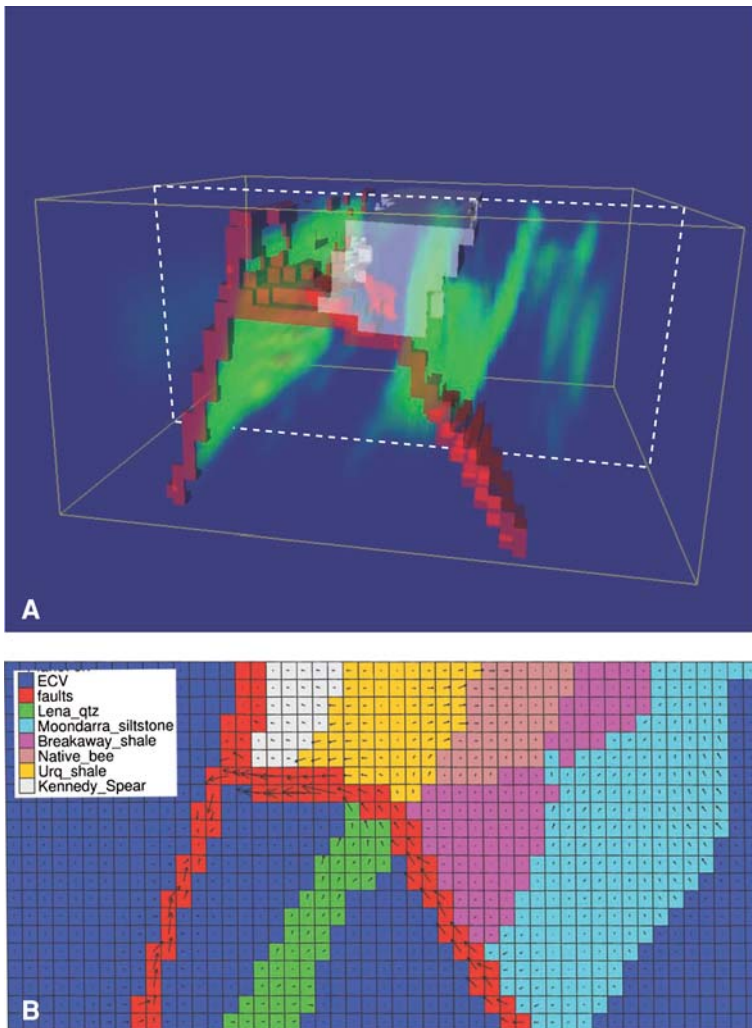


Fig. 8 Oblique strike slip scenario at $\psi_{\text{vertical}} = 0.68^\circ$ and $\psi_{\text{horizontal}} = 0.86^\circ$. **a** Strain patterns where *green* is maximum, low values are rendered transparent. Notice reactivation of Mount Isa fault (*steep red* structure). Extent of Urquhart shale is shown in semi-transparent *white*; position of cross section in **b** is shown by *white dotted* line. View is towards N. **b** Flow patterns in oblique strike slip show upward flow in the Paroo fault towards the Mount Isa fault, and lateral flow in the Urquhart shale

pattern is more complex than in the contraction case, with flow up the Paroo fault toward the Mount Isa fault, and out of the Urquhart shale. Maximal flow rates are $3.4 \times 10^{-8} \text{ ms}^{-1}$ (ca. 1 m/year).

3. In *extension* simulations normal sense shear zones form along the lower part of the Paroo fault, and transect the Isa Group in the eastern part of the model. A normal sense (west side down) shear zone also reactivates the Mount Isa fault (Fig. 9). Downward flow is due to tensile stresses, which lead to an overall drop in solid and fluid pressures,

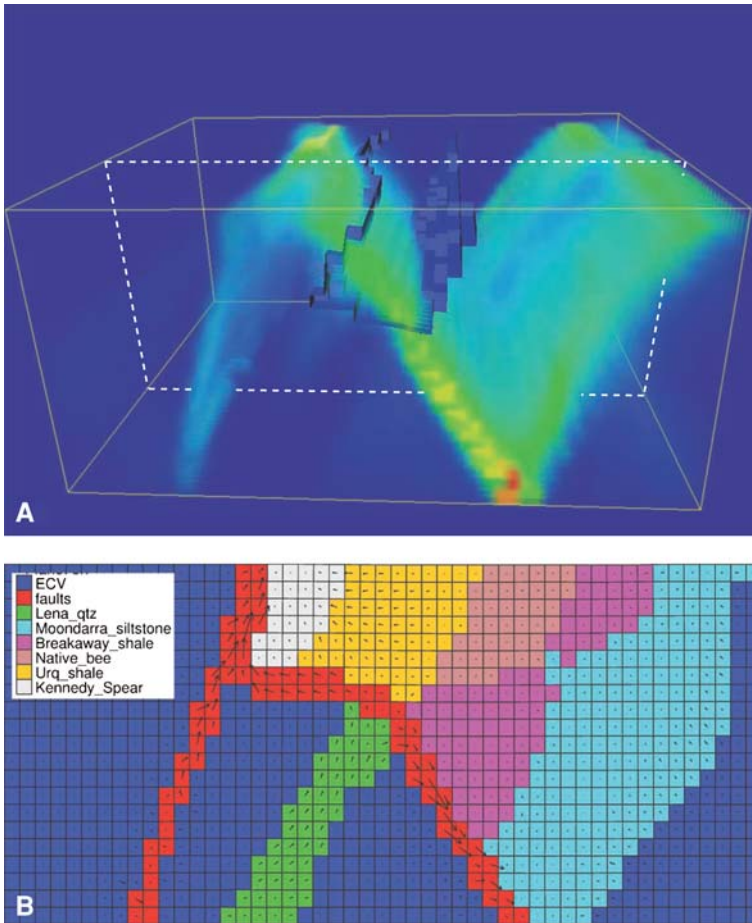


Fig. 9 Extension scenario at 5% strain. **a** Shear strain pattern where *red* is maximum and low values are *green* to transparent. Notice weak reactivation of the Mount Isa fault in the left third of image. Boundaries of Urquhart shale are shown in *blue*; position of cross section in **b** is shown by *white dotted line*. View is towards N and down. **b** Flow pattern in extension. Notice overall downward flow, except in lower part of Mount Isa fault and Lena Quartzite (*green*) View is towards N

even if the model is initialised with an above-hydrostatic fluid pressure gradient. The maximal flow velocity is $1.8 \times 10^{-7} \text{ ms}^{-1}$ (ca. 6 m/year).

4. In *top-to-E simple shear* simulations a shear zone forms along the flat part of the Paroo fault below the Urquhart shale (Fig. 10), at the approximate orientation and depth level of a massive dilation zone in the mine, the Buck Quartz fault. Fracturing, as inferred from shearing along the anisotropy orientation initiates in the lower part of the Urquhart shale, which corresponds to the shear strain maximum near the flat part of the Paroo fault. The flow pattern shows upward flow in the Urquhart shale and the Paroo fault, and fluid feeding into the Paroo from the Mount Isa fault. The maximal flow velocity is $5 \times 10^{-8} \text{ ms}^{-1}$ (ca. 3.5 m/year).

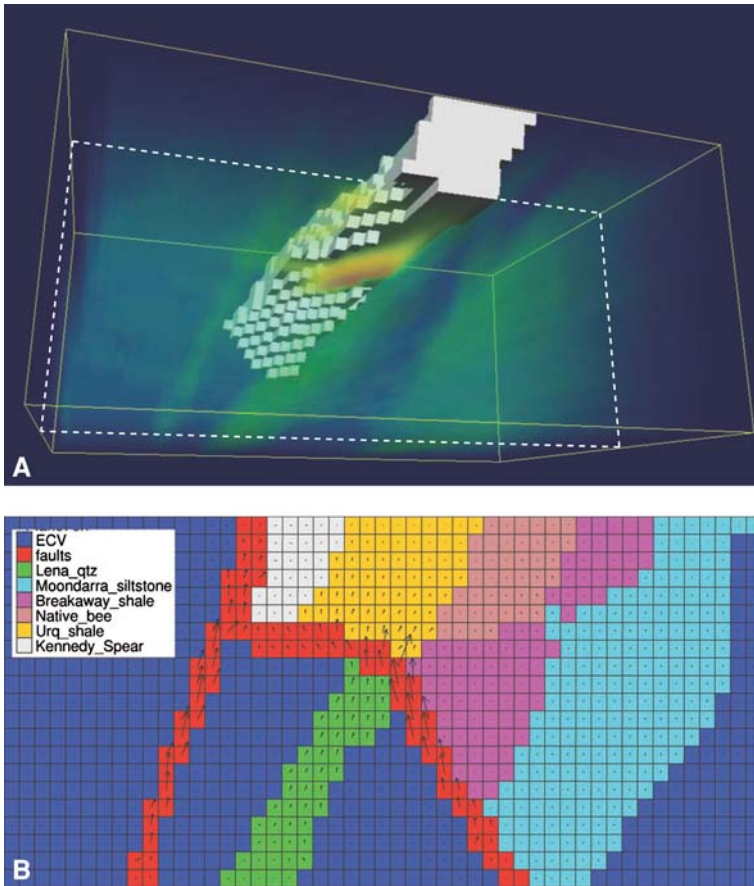


Fig. 10 Simple shear scenario. **a** Shear strain pattern in simple shear, where *red* is maximum, low values are *green* to transparent. Notice flat, near horizontal shear zone at flat part of Paroo fault; position of cross section in **b** is shown by *white dotted line*. View is towards NNE, from below; Urquhart shale is shown as a *grey box*. **b** Flow pattern in top-to-E simple shear showing downward flow in the Urquhart shale and the Paroo Fault. View is towards N

3.5 Structural Controls on Mineralisation

Coupled deformation and fluid flow simulations suggest that localization of strain and fracturing in the Urquhart shale most likely occurred in contraction, simple shear, and during oblique strike slip movement. In contraction the occurrence of a strain maximum in the lower part of the Urquhart shale represents a good fit with field observations, and the upward flow of fluid could be related to infiltration of a basement equilibrated reduced fluid (Wilde et al. 2005; Kendrick et al. 2007). In oblique slip dilation occurs along steep structures, which could favour infiltration of a surface fluid, or mixing between a metamorphic fluid and a fluid from a shallow crustal source (Kendrick et al. 2007). The strain and flow pattern generated in extension represents a poor match with field observations, suggesting that this scenario is not relevant. The inferred fracture pattern in simple shear (Fig. 11) fits the extent of the breccia zone in the copper mine very well, and suggests that

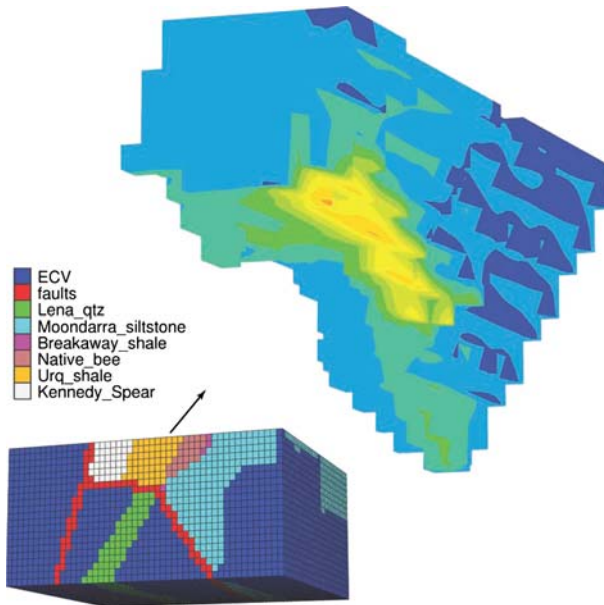


Fig. 11 Evolving strain (and inferred fracturing) pattern in strike-slip in directionally weak Urquhart shale shows similarity to mineralisation in Fig. 5. View from below, towards NW

a component of top-to East directed simple shear (D_3) is likely to have been involved in the formation of the fracture zone.

3.6 What Caused Fluid Flow?

In the case of Mount Isa the processes driving fluid flow are not clear. To generate the massive silica alteration observed in the copper system the upward flow of a cooling, and possibly de-pressurising silica-bearing fluid is likely. Hydraulic head driven flow (Garven and Ruffensperger 1997) is one possible scenario; free thermal convection is another likely possibility along with transient upward flow of overpressured fluid due to the breaching of a seal, both of which will be discussed elsewhere (Kühn and Gessner 2009a, b—this volume). Irrespective of what the processes driving fluid flow may have been, our models suggest that rocks of contrasting strength in proximity to reactivated faults provided the potential for localisation of deformation and the generation of permeability, thus exerting a structural control on where the ore bodies formed. The increased permeability in substantial parts of the Urquhart shale provided large volumes of permeable rock, which exceeded the relatively small volume of permeable faults in the system by large amounts. The change from regional contraction and simple-shear to strike-slip changed the hydraulic architecture significantly, favouring upward flow, lithostatic fluid pressures and hydrofracturing in the former case, and access to surface-derived fluids in the latter.

4 Conclusions

Hydromechanical coupling plays an important role in the generation of permeability in tectonic deformation. In the brittle-plastic part of the Earth's crust the coupling of

Mohr–Coulomb plasticity with Darcy flow in a continuum model can be used to simulate fluid flow in hydrothermal mineral systems. This technique has been used to model the Mesoproterozoic Mount Isa copper system, where deformation events reactivated a multiply deformed geological architecture during hydrothermal activity. In a post-metamorphic setting such as the Mount Isa Copper system, deformation was a key process to generate permeability. Contraction, oblique slip, and top-to East directed simple shear, or combinations of these, are likely to have occurred during alteration and mineralisation events. A transition from contraction to strike slip may have changed solid and fluid pressures on the scale of the hydrothermal system at Mount Isa. Pressure gradient driven upward flow would have favoured cooling and silica precipitation, which is a key feature of the Mount Isa system.

Acknowledgments The author wishes to thank Xstrata Copper Australia, who funded this research through the Predictive Mineral Discovery Cooperative Research Centre (*pmd**CRC) and provided generous logistical support. A. R. Wilde, P. A. Jones, M. Gregory, R. Duncan, P. Gow, R. D. Wilson, D. A-Izzedin, M. McGough, A. Ord, L. Chapman, B. Perkins, J. Proffett, J. Walshe, P. Sorjonen-Ward and B. E. Hobbs are thanked for fruitful discussions. P. Schaub and O. Kolditz are thanked for constructive and helpful reviews.

References

- Ague JJ (2004) Fluid flow in the deep crust. In: Rudnick RL (ed) *The crust: treatise on geochemistry*, vol 3. Elsevier, Amsterdam, pp 195–228
- Aydin A, Johnson AM (1983) Analysis of faulting in porous sandstones. *J Struct Geol* 5:19–31. doi:10.1016/0191-8141(83)90004-4
- Bell TH, Hickey KA (1998) Multiple deformations with successive and subhorizontal axial planes in the Mount Isa Region: their impact on geometric development and significance for mineralization and exploration. *Econ Geol* 93:1369–1389
- Bell TH, Perkins WG, Swager CP (1988) Structural controls on development and localization of syntectonic copper mineralization at Mount Isa, Queensland. *Econ Geol* 83:69–85
- Betts PG, Giles D, Mark G, Lister GS, Goleby BR, Ailleres L (2006) Synthesis of the Proterozoic evolution of the Mount Isa Inlier. *Aust J Earth Sci* 53:187–211. doi:10.1080/08120090500434625
- Biot MA (1956) Theory of deformation of a porous viscoelastic anisotropic solid. *J Appl Phys* 27:459–467. doi:10.1063/1.1722402
- Braun J, Munroe M, Cox SF (2003) Transient fluid flow in and around a fault. *Geofluids* 3:81–87. doi:10.1046/j.1468-8123.2003.00051.x
- Byerlee J (1978) Friction of rocks. *Pure Appl Geophys* 116:611–622
- Clauser C (1992) Permeability of crystalline rocks. *Eos Trans AGU* 73:233. doi:10.1029/91EO00190(237–238)
- Connors KA, Lister GS (1995) Polyphase deformation in the western Mount Isa Inlier, Australia: episodic or continuous deformation? *J Struct Geol* 17:305–328. doi:10.1016/0191-8141(94)00057-7
- Connors KA, Proffett JM, Lister GS, Scott RJ, Oliver NHS, Young DJ (1992) Geology of the Mount Novit ranges, southwest of Mount Isa mine. *Aust Bur Miner Resour Bull* 243:137–160
- Cook AM, Myer LR, Cook NGW, Doyle FM (1990) The effects of tortuosity on flow through a natural fracture. *Proc Symp Rock Mech* 31:371–378
- Coulomb CA (1773) *Sur une application des règles de Maximix et Minimis a quelques problèmes de statique relatifs à l'Architecture*. Academie Royale des Sciences Memoires de mathematique et de physique par divers savans 7:343–382
- Cox SF (2005) Coupling between deformation, fluid pressures, and fluid flow in ore-producing hydrothermal systems at depth in the crust. In Skinner BJ (ed) *Economic geology 100th anniversary volume*, pp 39–75
- Cox SF, Ruming K (2004) The St Ives mesothermal gold system, Western Australia—a case of golden aftershocks? *J Struct Geol* 26:1109–1125. doi:10.1016/j.jsg.2003.11.025
- Cox SF, Knackstedt MA, Braun J (2001) Principles of structural control on permeability and fluid flow in hydrothermal systems. In Richards JP, Tosdal RM (eds) *Structural controls on ore genesis*, pp 1–24

- Cundall P, Board M (1988) A microcomputer program for modelling large-strain plasticity problems International Conference on Numerical Methods in Geomechanics Abstracts. Innsbruck (Austria)
- Edmond JM, Paterson MS (1972) Volume changes during the deformation of rocks at high pressures. *Int J Rock Mech Min Sci* 9:161–182. doi:[10.1016/0148-9062\(72\)90019-8](https://doi.org/10.1016/0148-9062(72)90019-8)
- Etheridge MA, Wall VJ, Cox SF, Vernon RH (1984) High fluid pressures during regional metamorphism and deformation; implications for mass transport and deformation mechanisms. *J Geophys Res* 89(B6):4344–4358
- Fischer GJ, Paterson MS (1989) Dilatancy during rock deformation at high-temperatures and pressures. *J Geophys Res-Solid Earth Planet* 94:17607–17617. doi:[10.1029/JB094iB12p17607](https://doi.org/10.1029/JB094iB12p17607)
- Fisher QJ, Knipe RJ (1998) Fault sealing processes in siliciclastic sediments. *Geol Soc Spec Publ* 147:117–134. doi:[10.1144/GSL.SP.1998.147.01.08](https://doi.org/10.1144/GSL.SP.1998.147.01.08)
- Garven G, Raffensperger JP (1997) Hydrogeology and geochemistry of ore genesis in sedimentary basins. Wiley, New York
- Gessner K, Jones PA, Wilde AR, Kühn M (2006) Significance of strain localization and fracturing in relation to hydrothermal mineralization at Mount Isa, Australia. *J Geochem Explor* 89:129–132. doi:[10.1016/j.gexplo.2005.11.048](https://doi.org/10.1016/j.gexplo.2005.11.048)
- Ghassemi A, Tarasovs S, Cheng AHD (2007) A 3-D study of the effects of thermomechanical loads on fracture slip in enhanced geothermal reservoirs. *Int J Rock Mech Min Sci* 44:1132–1148. doi:[10.1016/j.ijrmm.2007.07.016](https://doi.org/10.1016/j.ijrmm.2007.07.016)
- Gow PA, Upton P, Zhao C, Hill KC (2002) Copper-gold mineralisation in New Guinea; numerical modelling of collision, fluid flow and intrusion-related hydrothermal systems. *Aust J Earth Sci* 49:753–771
- Gregory M, Keays RR, Wilde AR, Schaefer BF (2005) Preliminary Re-Os dating of the Mount Isa copper ores, Northwest Queensland. *Geochim Cosmochim Acta* 69:A569–A569
- Handin J, Hager RV, Friedman M, Feather JN (1963) Experimental deformation of sedimentary rocks under confining pressure; pore pressure tests. *AAPG Bull* 47:717–755
- Heinrich CA, Bain JHC, Fardy JJ, Waring CL (1993) Br/Cl geochemistry of hydrothermal brines associated with Proterozoic metasediment-hosted copper mineralization at Mount Isa, northern Australia. *Geochim Cosmochim Acta* 57:2991–3000. doi:[10.1016/0016-7037\(93\)90288-8](https://doi.org/10.1016/0016-7037(93)90288-8)
- Hobbs BE, Mühlhaus H-B, Ord A (1990) Instability, softening and localization of deformation. In Knipe RJ, Rutter EH (eds) Deformation mechanisms, rheology and tectonics, pp 143–165
- Holyland PW, Ojala VJ (1997) Computer-aided structural targeting in mineral exploration: two- and three-dimensional stress mapping. *Aust J Earth Sci* 44:421–432. doi:[10.1080/08120099708728323](https://doi.org/10.1080/08120099708728323)
- Hubbert MK, Rubey WW (1959) Mechanics of fluid-filled porous solids and its application to overthrust faulting. [Part] 1 of Role of fluid pressure in mechanics of overthrust faulting. *Geol Soc Am Bull* 70:115–166. doi:[10.1130/0016-7606\(1959\)70\[115:ROFPIM\]2.0.CO;2](https://doi.org/10.1130/0016-7606(1959)70[115:ROFPIM]2.0.CO;2)
- Itasca (2000) FLAC (Fast Lagrangian Analysis of Continua) Itasca Consulting Group, Minneapolis
- Itasca (2003) FLAC3D (Fast Lagrangian Analysis of Continua in Three Dimensions) Itasca Consulting Group, Minneapolis
- Jaeger JC, Cook NGW (1979) Fundamentals of rock mechanics. Methuen, London
- Jiang Z, Oliver NHS, Barr TD, Power WL, Ord A (1997) Numerical modeling of fault-controlled fluid flow in the genesis of tin deposits of the Malage ore field, Gejiu mining district, China. *Econ Geol* 92:228–247
- Kendrick MA, Mark G, Phillips D (2007) Mid-crustal fluid mixing in a Proterozoic Fe oxide-Cu-Au deposit, Ernest Henry, Australia: Evidence from Ar, Kr, Xe, Cl, Br, and I. *Earth Planet Sci Lett* 256:328–343. doi:[10.1016/j.epsl.2006.12.032](https://doi.org/10.1016/j.epsl.2006.12.032)
- Kolditz O, Clauser C (1998) Numerical simulation of flow and heat transfer in fractured crystalline rocks: Application to the Hot Dry Rock site in Rosemanowes (UK). *Geothermics* 27:1–23. doi:[10.1016/S0375-6505\(97\)00021-7](https://doi.org/10.1016/S0375-6505(97)00021-7)
- Kühn M, Gessner K (2009) Coupled process models of fluid flow and heat transfer in hydrothermal systems in three dimensions. *Surv Geophys*. doi:[10.1007/s10712-009-9060-8](https://doi.org/10.1007/s10712-009-9060-8)
- Kühn M, Gessner K (2009) Testing hypotheses for the Mount Isa Copper mineralisation with numerical simulations. *Surv Geophys* (in press)
- Mair JL, Ojala VJ, Salier BP, Groves DI, Brown SM (2000) Application of stress mapping in cross-section to understanding ore geometry, predicting ore zones and development of drilling strategies. *Aust J Earth Sci* 47:895–912. doi:[10.1046/j.1440-0952.2000.00814.x](https://doi.org/10.1046/j.1440-0952.2000.00814.x)
- Mandl G (1988) Mechanics of Tectonic Faulting. Models and basic concepts, Elsevier, Amsterdam
- Marti J, Cundall PA (1982) Mixed discretization procedure for accurate modelling of plastic collapse. *Int J Numer Anal Methods Geomech* 6:129–139. doi:[10.1002/nag.1610060109](https://doi.org/10.1002/nag.1610060109)

- Matthäi SK, Roberts SG (1997) Transient versus continuous flow in seismically active faults: an investigation by electric analogue and numerical modelling In: Jamtveit B, Yardley BWD (eds) Fluid flow and transport in rocks. Chapman and Hall, London, pp 263–296
- McLellan JG, Oliver NHS, Schaub PM (2004) Fluid flow in extensional environments; numerical modelling with an application to Hamersley iron ores. *J Struct Geol* 26:1157–1171. doi:[10.1016/j.jsg.2003.11.015](https://doi.org/10.1016/j.jsg.2003.11.015)
- Micklethwaite S, Cox SF (2004) Fault-segment rupture, aftershock-zone fluid flow, and mineralization. *Geology* 32:813–816. doi:[10.1130/G20559.1](https://doi.org/10.1130/G20559.1)
- Mohr CO (1900) Welche Umstände bedingen die Elastizitätsgrenze und den Bruch eines Materials? *Z Vereins Deutscher Ingenieure* 24:1524–1530
- Neuzil CE (2003) Hydromechanical coupling in geologic processes. *Hydrogeol J* 11:41–83
- Nguyen PT, Cox SF, Harris LB, Powell CM (1998) Fault-valve behaviour in optimally oriented shear zones; an example at the Revenge gold mine, Kambalda, Western Australia. *J Struct Geol* 20:1625–1640. doi:[10.1016/S0191-8141\(98\)00054-6](https://doi.org/10.1016/S0191-8141(98)00054-6)
- Ojala VJ, Ridley JR, Groves DI, Hall GC (1993) The Granny Smith gold deposit—the role of heterogeneous stress-distribution at an irregular granitoid contact in a Greenschist Facies Terrane. *Miner Depos* 28:409–419. doi:[10.1007/BF02431599](https://doi.org/10.1007/BF02431599)
- Oliver NHS, Bons P (2001) Mechanisms of fluid flow and fluid–rock interaction in fossil metamorphic hydrothermal systems inferred from vein–wallrock patterns, geometry and microstructure. *Geofluids* 1:137–162. doi:[10.1046/j.1468-8123.2001.00013.x](https://doi.org/10.1046/j.1468-8123.2001.00013.x)
- Oliver NHS, Ord A, Valenta RK, Upton P (2001) Deformation, fluid flow and ore genesis in heterogeneous rocks with examples and numerical models from the Mount Isa District, Australia. In Richards JP, Tosdal RM (eds) Structural controls on ore genesis. Society of Economic Geologists, Inc., pp 51–74
- Ord A (1990) Mechanical control on dilatant shear zones In: Knipe RJ, Rutter EH (eds) Deformation mechanisms, rheology and tectonics. pp 183–192
- Ord A, Oliver NHS (1997) Mechanical controls on fluid flow during regional metamorphism; some numerical models. *J Metamorph Geol* 15:345–359. doi:[10.1111/j.1525-1314.1997.00030.x](https://doi.org/10.1111/j.1525-1314.1997.00030.x)
- Ord A, Hobbs BE, Zhang Y, Broadbent GC, Brown M, Willetts G, Sorjonen-Ward P, Walshe JL, Zhao C (2002) Geodynamic modelling of the Century deposit, Mt Isa Province, Queensland. *Aust J Earth Sci* 49:1011–1039. doi:[10.1046/j.1440-0952.2002.00968.x](https://doi.org/10.1046/j.1440-0952.2002.00968.x)
- Paterson MS, Wong TF (2005) Experimental rock deformation—the brittle field. Springer, Berlin
- Perkins WG (1984) Mount Isa silica dolomite and copper orebodies; the result of a syntectonic hydrothermal alteration system. *Econ Geol* 79:601–637
- Potma W, Roberts PA, Schaub PM, Sheldon HA, Zhang Y, Hobbs BE, Ord A (2008) Predictive targeting in Australian orogenic-gold systems at the deposit to district scale using numerical modelling. *Aust J Earth Sci* 55:101–122. doi:[10.1080/08120090701673328](https://doi.org/10.1080/08120090701673328)
- Robinson JA, Wilson CJL, Rawling TJ (2006) Influence of volcano-sedimentary facies architecture on strain partitioning during the evolution of an orogenic-gold lode system, Stawell, western Victoria. *Aust J Earth Sci* 53:721–732. doi:[10.1080/08120090600827413](https://doi.org/10.1080/08120090600827413)
- Rutqvist J, Stephansson O (2003) The role of hydromechanical coupling in fractured rock engineering. *Hydrogeol J* 11:7–40
- Schaub PM, Zhao C (2002) Numerical models of gold-deposit formation in the Bendigo-Ballarat Zone, Victoria. *Aust J Earth Sci* 49:1077–1096. doi:[10.1046/j.1440-0952.2002.00964.x](https://doi.org/10.1046/j.1440-0952.2002.00964.x)
- Schaub PM, Rawling TJ, Dugdale LJ, Wilson CLJ (2006) Factors controlling the location of gold mineralisation around basalt domes in the stawell corridor: insights from coupled 3D deformation—fluid-flow numerical models. *Aust J Earth Sci* 53:841–862
- Secor DT (1965) Role of fluid pressure in jointing. *Am J Sci* 263:633–646
- Secor DT, Pollard DD (1975) On the stability of open hydraulic fractures in the Earth's crust. *J Geophys Res* 2:510–513
- Sheldon HA, Micklethwaite S (2007) Damage and permeability around faults: implications for mineralization. *Geology* 35:903–906. doi:[10.1130/G23860A.1](https://doi.org/10.1130/G23860A.1)
- Sheldon HA, Ord A (2005) Evolution of porosity, permeability and fluid pressure in dilatant faults post-failure: implications for fluid flow and mineralization. *Geofluids* 5:272–288. doi:[10.1111/j.1468-8123.2005.00120.x](https://doi.org/10.1111/j.1468-8123.2005.00120.x)
- Sheldon HA, Barnicoat AC, Ord A (2006) Numerical modelling of faulting and fluid flow in porous rocks: an approach based on critical state soil mechanics. *J Struct Geol* 28:1468–1482. doi:[10.1016/j.jsg.2006.03.039](https://doi.org/10.1016/j.jsg.2006.03.039)
- Sibson RH (1994) Crustal stress, faulting and fluid flow. *Geol Soc Spec Publ* 78:69–84. doi:[10.1144/GSL.SP.1994.078.01.07](https://doi.org/10.1144/GSL.SP.1994.078.01.07)

- Sibson RH (2001) Seismogenic framework for hydrothermal transport and ore deposition. *Rev Econ Geol* 14:25–50
- Sorjonen-Ward P, Zhang Y, Zhao C (2002) Numerical modelling of orogenic processes and gold mineralisation in the southeastern part of the Yilgarn Craton, West Australia. *Aust J Earth Sci* 49:935–964. doi:[10.1046/j.1440-0952.2002.00969.x](https://doi.org/10.1046/j.1440-0952.2002.00969.x)
- Swager CP (1985) Syndeformational carbonate-replacement model for the copper mineralization at Mount Isa, Northwest Queensland; a microstructural study. *Econ Geol* 80:107–125
- Twiss RJ, Moores EM (1992) Structural geology. W.H. Freeman, San Francisco
- Vermeer PA, de Borst R (1992) Non-associated plasticity for soils, concrete and rock. *Heron* 29:1–65
- Vos IMA, Potma W, Bierlein FP, Sheldon HA (2007) Numerical modelling of the western Hodgkinson Province, northeast Queensland: implications for gold mineralisation. *Aust J Earth Sci* 54:27–47. doi:[10.1080/08120090600981434](https://doi.org/10.1080/08120090600981434)
- Wilde AR, Gregory M, Duncan R, Gessner K, Kühn M, Jones PA (2005) Geochemical process model for the Mt Isa Cu–Co–Ag deposits. In: Bierlein FP, Mao J (eds) *Mineral deposit research: meeting the global challenge*. Springer, Berlin, pp 199–202
- Yardley BWD, Baumgartner LP (2007) Fluid processes in deep crustal fault zones. In: Handy MR, Hirth G, Hovius N (eds) *Tectonic faults: agents of change on a dynamic Earth*. MIT Press, Cambridge, pp 295–318
- Zhang SQ, Paterson MS, Cox SF (1994) Porosity and permeability evolution during hot isostatic pressing of calcite aggregates. *J Geophys Res* 99:15741–15760. doi:[10.1029/94JB00646](https://doi.org/10.1029/94JB00646)
- Zhang Y, Sorjonen-Ward P, Ord A (2006a) Modelling fluid transport associated with mineralization and deformation in the Outokumpu Cu–Zn–Co deposit, Finland. *J Geochem Explor* 89:465–469. doi:[10.1016/j.gexplo.2005.11.035](https://doi.org/10.1016/j.gexplo.2005.11.035)
- Zhang Y, Sorjonen-Ward P, Ord A, Southgate PN (2006b) Fluid flow during deformation associated with structural closure of the Isa superbasin at 1575 Ma in the central and northern Lawn Hill platform, northern Australia. *Econ Geol* 101:1293–1312. doi:[10.2113/gsecongeo.101.6.1293](https://doi.org/10.2113/gsecongeo.101.6.1293)
- Zhang YH, Lin G, Roberts P, Ord A (2007) Numerical modelling of deformation and fluid flow in the Shuikoushan district, Hunan Province, South China. *Rev Econ Geol* 31:261–278